Journal of Materials Chemistry C

RSC Publishing

PAPER

View Article Online
View Journal

Cite this: DOI: 10.1039/c3tc31819b

Resistive switching dependence on atomic layer deposition parameters in HfO_2-based memory devices†

Raúl Zazpe,[a] Mariana Ungureanu,[a] Federico Golmar,[ab] Pablo Stoliar,‡[acd] Roger Llopis,[a] Fèlix Casanova,[ae] David F. Pickup,[fg] Celia Rogero[fh] and Luis E. Hueso*[ae]

Received 13th September 2013
Accepted 22nd October 2013

DOI: 10.1039/c3tc31819b

www.rsc.org/MaterialsC

Resistance random access memory (ReRAM) is considered a promising candidate for the next generation of non-volatile memory. In this work, we fabricate Co/HfO_2/Ti devices incorporating atomic-layer-deposited HfO_2 thin films as the active material grown under different atomic layer deposition (ALD) conditions. We focus on analyzing the effect of ALD conditions on the resistive switching behaviour of the devices. Electrical characterization reveals a particular non-crossing current–voltage curve and bipolar resistive switching behaviour. Device memory properties were confirmed by stability and retention measurements as well as voltage pulses, by which logical computational processes were conducted. X-ray photoelectron spectroscopy combined with electrical measurements demonstrates that the presence of Hf sub-oxides at the interface with the underlying Ti layer is required in order to achieve a stable switching device. The ability of Ti to scavenge oxygen from the HfO_2 is shown to be affected by the ALD conditions.

Introduction

Different candidates[1] are being developed with the objective of becoming the core of the next non-volatile memory (NVM) generation. Properties such as short access time (<200 ns), long lifetime (10^9 to 10^{12} cycles for writing/erasing and reading processes respectively), low cost (<1 $ per GB), and low operation power (μW) are considered compulsory for new technologies to become competitive. Resistance random access memory (ReRAM), based on the resistive switching (RS) phenomenon, has emerged amongst the most promising candidates for new NVM.[2,3] The ReRAM memory cell usually has a metal/insulator/metal (MIM) capacitor structure in which an insulating oxide is sandwiched between two metal electrodes, while its operation is based on the reversible voltage-induced switching between two stable resistance states. ReRAM devices based on different transition metal oxides, such as $SrTiO_3$,[4–7] NiO,[8–10] TiO_2 (ref. 11–13) and ZnO,[14–16] have been reported. Hafnium oxide (HfO_2) has also been studied[17–22] mainly due to its well-known fabrication technology, its good thermodynamic stability and its high breakdown electric field. In this work we fabricate MIM HfO_2-based devices, which have the structure highlighted in Fig. 1a, and study the effect of the oxide deposition conditions on their RS behavior. Electrical characterization is carried out revealing unusual non-crossing current (I)–voltage (V) curves at the origin and non-volatile memory properties. We present a parameter diagram in which the occurrence of the switching events is related to two different deposition parameters, namely the nitrogen purge time and the deposition temperature. X-ray photoelectron spectroscopy (XPS) is used to investigate the origin of differing RS performance with respect to the device

[a]CIC nanoGUNE Consolider, Tolosa Hiribidea 76, 20018 Donostia – San Sebastian, Basque Country, Spain. E-mail: l.hueso@nanogune.eu; Fax: + 34 943 57 4001; Tel: +34 943 57 4011

[b]I.N.T.I. – CONICET, Av. Gral. Paz 5445, Ed. 42, B1650JKA, San Martín, Bs As, Argentina

[c]LPS, CNRS UMR 8502, Université Paris Sud, Bât 510, 91405 Orsay, France

[d]ECyT, UNSAM, Martín de Irigoyen 3100, B1650JKA, San Martín, Bs As, Argentina

[e]IKERBASQUE, Basque Foundation for Science, 48011 Bilbao, Basque Country, Spain

[f]Material Physics Center (MPC), Centro de Física de Materiales (CSIC-UPV-EHU), 20018 San Sebastían, Spain

[g]Departamento de Física Aplicada I, Universidad del País Vasco, 20018 San Sebastián, Spain

[h]Donostia International Physics Center (DIPC), 20018 San Sebastián, Spain

† Electronic supplementary information (ESI) available. See DOI: 10.1039/c3tc31819b

‡ IMN, Université de Nantes, CNRS, 44322 Nantes, France.

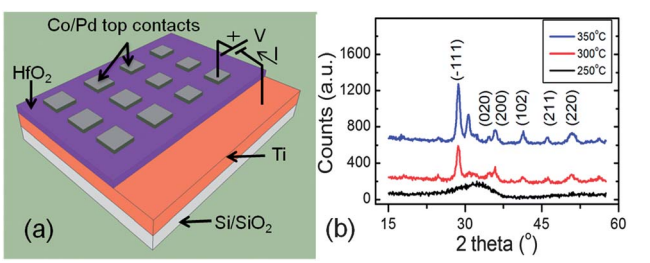

Fig. 1 (a) Schematic diagram and electrical configuration of a typical Co/HfO_2/Ti sample with an array of devices. (b) X-Ray diffraction spectra from HfO_2 thin films grown at 250 °C, 300 °C and 350 °C. Labels indicate the main plane reflections of the monoclinic phase.

composition. Results revealed that the presence of Hf sub-oxides (oxygen vacancies) was required at the HfO_2/Ti interface in order to achieve resistive switching. Generation of these oxygen vacancies is attributed to the strong oxygen gettering potential of the underlying Ti layer, which is found to be dependent on the atomic layer deposition (ALD) conditions. Such correlation between the XPS results and the RS performance provides information on the switching mechanism.

Experimental methods

Arrays of Co/HfO_2/Ti devices (16 × 5 devices) were fabricated on 10 × 10 mm p-type silicon substrates covered by 150 nm of thermally grown SiO_2. The common Ti bottom electrode (20 nm thick) was deposited by sputtering. Subsequently, HfO_2 films (20 nm thick) were deposited by ALD[23–25] using H_2O vapour as an oxidant and tetrakis(dimethylamino)hafnium (TDMAH) as the Hf precursor in alternating pulses. Nitrogen was used as the carrier and purging gas of the reaction in between pulses. The films were grown with different purge times (from 1 to 35 seconds) and deposition temperatures (from 125 °C to 350 °C). The purge time can be defined as the delay time in between two consecutive pulses where an inert gas purges the chamber to eliminate unreacted precursors and by-products of the process.[26] Finally, 35 nm thick Co top metal electrodes capped with Pd (200 × 200 μm^2) were deposited by photolithography and sputtering. The thicknesses and structural properties of the HfO_2 thin films were determined by reflectivity measurements and grazing incidence X-ray diffraction respectively. The peaks observed for samples grown at 300 °C and above result from a monoclinic phase,[25,27] with the exception of the reflection peak corresponding to a 2θ value of 30.6 attributed to the orthorhombic polymorph of HfO_2.[27] Whereas an amorphous structure was found at lower deposition temperatures as displayed in Fig. 1b.

Electrical characterization was performed at a probe station and involved current–voltage (*I–V*) sweeps, voltage pulse application, minor loops, and stability and retention measurements using a Keithley 2635A source meter controlled by custom computer software. The top and bottom electrodes were biased and grounded, respectively (see Fig. 1a for a schematic representation of a typical array of devices).

XPS experiments were performed using a Phoibos photoelectron spectrometer equipped with an Al Kα X-ray source (16 mA, 12.5 kV) as the incident photon radiation. The overall resolution of the instrument was approximately 0.9 eV. At this resolution the line energy positions could be determined with an accuracy better than ±0.2 eV. The pressure in the analyzing chamber was $<1.0 \times 10^{-9}$ mBar during measurements. Tantalum foil was used to create an electrical contact between the sample surface and the sample holder to avoid charging effects. Calibration of the binding energy scale was performed by fixing the adventitious C 1s peak to a value of 284.8 eV. CasaXPS software (version 2.3.15) was used to analyze the sample spectra.[28] A Shirley type baseline was employed and Gaussian (70%)–Lorentzian (30%) (GL(30)) profiles were used to fit the individual components. The background has been subtracted in the spectra detailed in the figures. Depth profiles of the deposited films were acquired by conducting XPS measurements after each argon ion beam etching cycle. To avoid any significant preferential sputtering and/or surface roughness the use of an argon beam at grazing incidence and very mild sputtering conditions were employed (1 keV for 10 minutes) during depth profiling analysis.[29] These conditions resulted in the removal of 3–4 nm of material during each cycle, a sputter rate of 0.3–0.4 nm min^{-1}.

Results and discussion

We report the effect of the deposition process conditions on the bipolar resistive switching behavior exhibited by Co/HfO_2/Ti devices. With the aim of changing the electronic properties of the insulating material, we intentionally fabricated 26 samples within a range of deposition temperatures (from 125 to 350 °C) and purge times (from 1 to 35 seconds). Fig. 2a shows a characteristic *I–V* curve displayed by a hysteretic Co/HfO_2/Ti device (HfO_2 grown at 300 °C and with 5 seconds purge time) where the dc voltage sweep is as follows: 0 V → 15 V → 0 V → −15 V → 0 V. The devices exhibit two different resistance states, a high resistance state (HRS) and a low resistance state (LRS) that can be alternated upon the application of an electric field. The process in which the device is switched from the HRS to the LRS is known as SET. In the pristine state the device exhibits a high resistance state (HRS) independent of the voltage bias polarity. A typical forming procedure is not required in these samples and the voltage value at which the first SET process occurs is basically the same as that observed for the subsequent SET processes. A significant characteristic displayed by the *I–V*

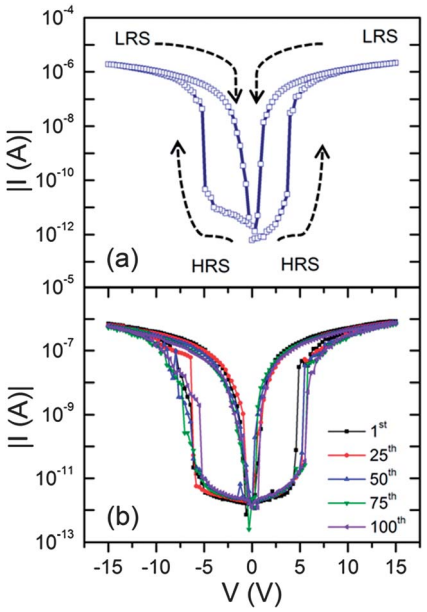

Fig. 2 (a) Typical experimental current (*I*)–voltage (*V*) curve for the Co/HfO_2/Ti device with deposition conditions for HfO_2, 300 °C and 5 seconds purge time. The dotted lines indicate the direction of the *I–V* curve. (b) Consecutive experimental *I–V* curves measured in the same device.

curve is the change of the resistive state sensed (from LRS to HRS) as the bias polarity is reversed as shown in Fig. 2a. This behavior results in a particular non-crossing *I–V* curve at the origin, where the two branches of the hysteresis curve do not intersect, instead of the characteristic self-crossing *I–V* curve at zero bias exhibited by materials displaying bipolar RS.[30] In Fig. 2a the device is in HRS as a positive voltage is applied until it switches to a low resistance state (LRS) at ≈+4.5 V (V_{SET}) through the SET process, in which an abrupt change in the resistance state of more than 3 orders of magnitude occurs. The device preserves the LRS during the rest of the positive branch of the *I–V* curve resulting in the hysteretic curve observed. However as bias voltage is reversed the device is in HRS, exhibiting similar behavior to that observed at the positive branch, and switches to LRS at ≈−5.5 V (V_{SET}) preserving such resistance states until the bias returns back to zero volts. The I_{LRS} values are lower than 10 μA, suggesting voltage power consumption in the μW regime. The device robustness, the *I–V* curve reproducibility and the stability of both V_{SET} values were revealed after conducting a significant number of cycles (>100) as shown in Fig. 2b.

Minor loops were performed in order to acquire a deeper understanding of the observed non-crossing *I–V* curve and of the memory retention. A minor loop consists of the application of a voltage sweep as follows: 0 V → 15 V → *A* → 15 V → 0 V, where *A* is a variable voltage value. In this work, the *A* voltage values applied were: 0, −1, −2 and −3 V. The measurements began with the device in an initial HRS, which was switched to the LRS as shown by path 1 in Fig. 3a. When the voltage was then swept back to zero volts (path 2), it resulted in an increase of the resistance state of the device as shown by subsequent path 3. The decrease of resistance increases with increasing applied voltage (see, for example, Fig. 3b and c). As the voltage was swept to more negative values the resistance state during the initial stages of path 3 became more robust until, when the voltage was swept until −3 V (Fig. 3e), the initial HRS was recovered. This means that a voltage value of opposite polarity with respect to the SET process is required to produce the RESET process, as reflected in Fig. 3b–e, indicating a bipolar behavior. Comparable results were obtained when these measurements were conducted using the opposite polarity, as illustrated in Fig. S1 (see ESI†). The results suggested the existence of two set–reset processes that could point towards the presence of two independent switching processes, which could be attributed to the existence of two switchable metal/oxide interfaces. If this assumption were correct, it would indicate that at positive and negative bias polarity we would sense the resistance states of the two different metal/oxide junctions and it would account for the unusual non-crossing *I–V* curve. It would also allow us to discern at which bias polarity the SET processes for the two metal/oxide junctions occurred. Furthermore, the LRS of one junction would be concurrent with the HRS of the other junction at a given bias polarity, explaining the transition from LRS to HRS when the voltage bias polarity is switched.

In order to confirm the bipolar RS behavior that the minor loops suggested, we conducted a sequence of logical memory processes (writing, reading and erasing) through the application of voltage pulses. The voltage pulse results would also confirm whether the system possesses the required properties for potential application as a non-volatile memory device. The writing and erasing are the logical operations through which the device is switched to LRS and HRS respectively, while the reading operations are applied to sense the resistance state of the device (HRS or LRS). Fig. 4a shows the logical processes carried out by electrical voltage pulses (20 ms width) and the concomitant currents for the positive *I–V* branch. The writing pulse must be larger than the V_{SET} in order to induce switching to the LRS, whilst the reading pulse must be less than V_{SET} to prevent changes in the resistance state during sensing. On the other hand the erasing pulse should be of opposite bias to switch back to the HRS, if the bipolar RS presumption is correct. Finally a zero-volt pulse is applied in between consecutive logical steps to verify the non-volatility of the memory. In Fig. 4a the device is switched from the HRS to the LRS by a writing pulse (+13 V) and during the subsequent reading operation (pulse of +4 V) a meaningful current, denoting the LRS of the device, is sensed as shown in Fig. 4b. The next erasing pulse (−4 V) triggers the switching back to HRS, confirmed by the current sensed during the second reading operation. This

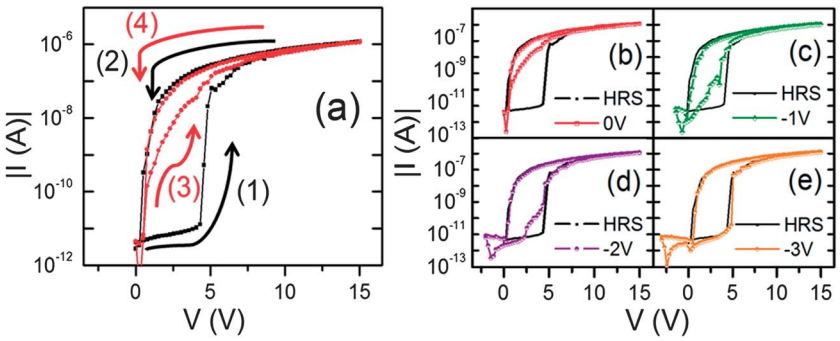

Fig. 3 (a) Minor loop data highlighting the SET process, for which the device switches from the HRS to the LRS (path 1), and the subsequent reverse sweep to 0 V (path 2). Path 3 shows a slight increase in the resistance state with respect to path 2, whereas the LRS returned in path 4. (b–e) Minor loops obtained for the positive branch of the *I–V* curve for the Co/HfO_2/Ti device (HfO_2 deposited at 300 °C and 5 seconds purge time) when applying the different *A* voltage values indicated in the legend. The SET and RESET processes occur at opposite polarity indicating bipolar resistive switching behavior.

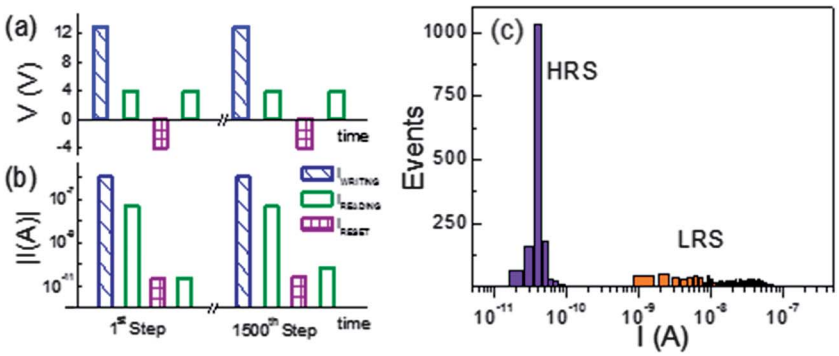

Fig. 4 Voltage pulse experimental data for a hysteretic Co/HfO_2/Ti device (HfO_2 grown at 300 °C and 5 seconds purge time). (a) Voltage applied and (b) the corresponding currents at the 1st and the 1500th pulse train. The writing step triggers the device to the LRS, confirmed by the current measured in the following reading step whilst the second reading current ratifies the return to the HRS produced by the erasing step. (c) Histogram of the 1500 reading current values obtained for the HRS and LRS.

sequence of pulses was carried out successfully more than 1.5×10^3 times without degeneration (1st and 1500th pulses shown in Fig. 4b), confirming the device capability as a non-volatile memory cell. The histogram of the reading current values for LRS and HRS obtained during the 1500 pulses is displayed in Fig. 4c. Their average values together with the standard deviation for HRS and LRS were $3.60 \times 10^{-11} \pm 1.00 \times 10^{-11}$ A, and $2.96 \times 10^{-8} \pm 2.07 \times 10^{-8}$ A, respectively. The HRS to LRS discrimination is close to 3 orders of magnitude; highlighting the negligible cross-reading between resistance states. Voltage pulse results also confirmed the bipolar nature of the resistive switching behavior exhibited by the device. Additionally, similar results were obtained when applying voltage pulses of opposite polarity. This substantiates the existence of two distinct SET–RESET operations that, at the same time, supports the existence of two independent switching processes in the device, associated with two active and switchable interfaces.

Further analysis of the memory properties was carried out with stability and retention experiments (see Fig. 5). Stability measurements consisted of setting the resistance state at either LRS or HRS and applying 400 successive reading steps (+4.2 V) in order to test the stability of such resistance states. It was carried out for both HRS and LRS for the positive branch. The histogram of the currents measured for both resistance states is shown in Fig. 5a. Their average current values for the HRS and the LRS were $1.97 \times 10^{-8} \pm 1.88 \times 10^{-8}$ A, and $8.67 \times 10^{-11} \pm 5.11 \times 10^{-12}$ A, respectively. On the other hand, retention analysis involved setting the device at either LRS or HRS and measuring uninterruptedly the current value under the application of a constant voltage value (+3.75 V) for a specific time (500 s). Fig. 5b shows the histogram obtained from the reading currents at both resistance states. Their average current values and the corresponding standard deviations for the HRS and LRS are $3.39 \times 10^{-11} \pm 6.46 \times 10^{-13}$ A and $1.23 \times 10^{-7} \pm 1.40 \times 10^{-8}$ A, respectively. The I_{LRS}/I_{HRS} ratios for stability and retention measurements were 2 and 3 orders of magnitude, respectively. The results from both stability and retention measurements exhibit no degradation of the resistance states, preserving a wide memory window.

The electrical characterization was carried out on each of the 26 samples fabricated under different conditions with the resulting statistics presented in the parameter diagram displayed in Fig. 6. For each sample type 10 different devices were characterized, showing a reproducibility of at least 80%. In order to determine the robustness of the hysteresis in the case of devices displaying RS, a reliability criterion was established. The criterion requires 150 successful switching *I–V* cycles for a device to be considered hysteretic, with the hysteresis of a

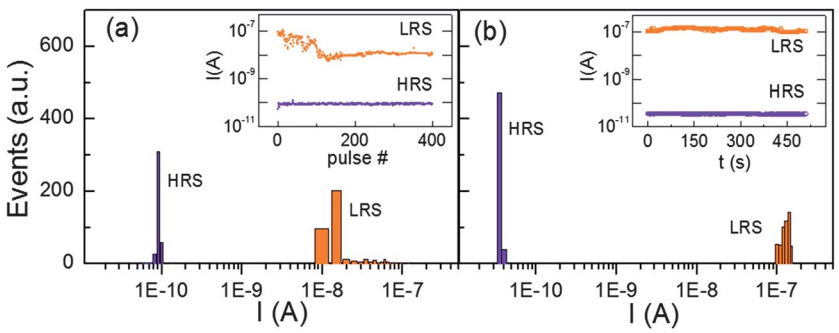

Fig. 5 Histogram of the reading current values obtained for the HRS and the LRS for (a) stability and (b) retention measurements of the Co/HfO_2/Ti device with HfO_2 deposition conditions of 300 °C and 5 seconds purge time. Inset (a): reading current values as a function of the number of pulses applied. Inset (b): reading current values as a function of time.

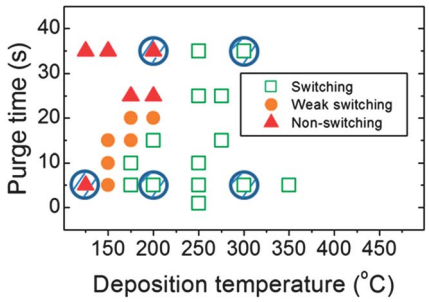

Fig. 6 Summary of resistive switching behavior (see text for definitions) obtained for samples fabricated at different deposition temperatures and purge times. The electrical characterization was carried out at 10 devices per sample in order to get reliable statistics to form the parameter diagram. The samples inside the patterned circles were analysed by XPS.

weakly hysteretic device fading away before achieving 150 cycles. The parameter diagram demonstrated the effect of the ALD conditions on the appearance of the RS phenomenon, indicating that reliable resistive switching seems to be supported by high deposition temperatures and short purge times. This trend allows us to confidently predict the RS behavior of a device as a function of the oxide deposition process conditions. The parameter diagram also revealed that samples with both amorphous and polycrystalline HfO_2 showed RS, ruling out direct correlation between the degree of HfO_2 crystallinity and RS performance.

The effect of both the purge time and the deposition temperature on the RS performance is shown in Fig. 7. Fig. 7a–e show the *I–V* curves for the hysteretic samples where the HfO_2 was grown at different deposition temperatures and a common purge time (5 s). Larger I_{LRS}/I_{HRS} ratios were found as the deposition temperature was increased, essentially due to an increase in the current associated with the LRS. On the other hand, the effect of different purge times at a given deposition temperature (200 °C) is shown in Fig. 7f. In this case an increased I_{LRS}/I_{HRS} ratio is observed when the purge time is shortened. These results would indicate that a more significant switch in resistance would be expected when the HfO_2 thin films are grown under certain conditions, *i.e.*, high temperatures together with short purge times.

For further understanding the switching properties of our HfO_2-based devices, we also performed electrical measurements in samples with bottom and top electrodes of different sizes. Electrode widths from 25 to 650 μm were fabricated in order to study the area dependence of the resistance. The electrical current measured at the LRS (with an applied voltage of 15 V) is roughly proportional to the electrode area (see Fig. 8), indicating that the whole metal/oxide interface is involved in the carrier transport process. Here we are simply assuming that the resistance of our device can be expressed as:

$$R = \frac{V}{I} = \frac{\rho t}{Lw}$$

where ρ is the resistivity of the HfO_2, t is the HfO_2 thin film thickness, L is the top electrode size and w is the bottom electrode width. This result would rule out filamentary conduction, in which case only a small area of the interface is involved in the LRS conduction.

As established above, the devices exhibit bipolar RS behaviour and the physical mechanism of this effect has been reported to be based on the interface energy barrier modification by the migration of oxygen.[2,31–35] This has also been previously described in the case of HfO_{2-x},[19,22,36] where oxygen vacancies produce a so-called sub-band in the HfO_{2-x} bandgap.[37–40] The trend observed in the parameter diagram (Fig. 6) together with the potential switching mechanism suggested by the literature led us to carry out XPS analysis.

In order to check for the presence of such vacancies in the HfO_2 we have performed XPS experiments on samples fabricated at different deposition temperatures and purge times (samples measured by XPS are marked with a circle in Fig. 6). As such, analysis was used to investigate how changing the HfO_2 atomic layer deposition conditions affected the chemical

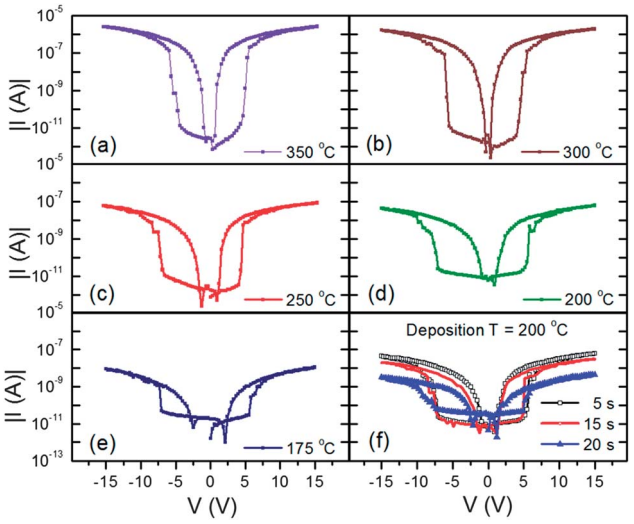

Fig. 7 Characteristic *I–V* curves reflect the effect on the RS of (a–e) the deposition temperature and (f) purge time during the growth of the HfO_2 thin films.

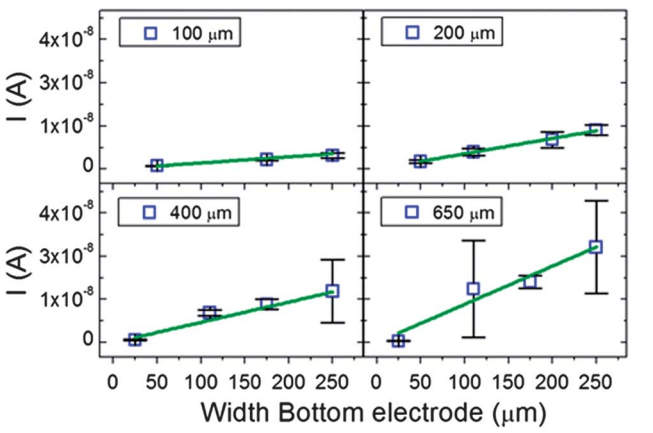

Fig. 8 Current sensed at 15 V *versus* the bottom electrode width for the four different top electrode sizes. The straight line corresponds to linear fitting of data.

properties of the deposited films and to deduce whether there was any systematic relationship with the observed resistive switching behavior. Fig. 9a shows Hf 4f XPS spectra from four different depths in the HfO_2 film for a hysteretic device (200 °C, 5 s purge time); near the surface (1 sputter cycle), in the bulk (3 sputter cycles), at the first detection of Ti (5 sputter cycles) and after a subsequent sputter (6 sputter cycles). The overall shape of the spectra exhibits two contributions associated with the two non-equivalent $4f_{7/2}$ and $4f_{5/2}$ core levels. Deconvolution of the spectra was carried out in order to ascertain which Hf species were present in the film. In all cases quantitative agreement was achieved between the Hf 4f assignment and that for the corresponding O 1s and N 1s spectra (data not shown). The spectra show that, near the surface and in the bulk, the film is predominantly composed of stoichiometric HfO_2 (red contributions in Fig. 9), which exhibits a Hf $4f_{7/2}$ peak at 17.1 eV, consistent with previous studies.[41–43] A second, much smaller contribution, from a lower BE component (Hf $4f_{7/2}$ at 15.9 eV), is assigned to a Hf–N species (blue components), possibly from HfN_x or HfO_xN_y.[42,44] These species could arise from the presence of the unreacted ALD precursor (tetrakis(dimethylamino) hafnium) or alternatively nitrogen could be incorporated into the film from the purge gas. XPS analysis is used to detail the relative N content found in HfO_2 films prepared under different deposition conditions (see Table S1 in the ESI†). The composition of the film remains almost constant until detection of the underlying Ti. This can be observed in the left panel of Fig. 9 but is further enhanced in Fig. S2 (see ESI†). The uniformity of the Hf 4f signal during depth profiling of the bulk (up to 4 sputter cycles) indicates that no significant preferential sputtering takes place, which has been the case when using the mild sputtering conditions employed here.[29] Upon sputtering down to the underlying Ti layer a noticeable change in the shape of the Hf 4f spectrum is observed, with a shift in peak position and less distinction between the two spin–orbit contributions (see Fig. S2, ESI†). This is due to the presence of a new component with a Hf $4f_{7/2}$ peak at 16.5 eV, which is associated with the presence of Hf suboxides[45] (green components). A summary of the peak positions of the different components used in the deconvolution of the Hf 4f data is given in Table S2 in the ESI.†

To determine whether the presence of these interfacial suboxides is important in order to achieve resistive switching Hf 4f XPS spectra at the HfO_2/Ti interface were acquired for hysteretic and non-hysteretic samples prepared under different conditions [spectrum (4) in Fig. 9a and all spectra in Fig. 9b]. Spectrum (A) is from a 200 °C, 35 s purged sample which yielded a non-switching device. The spectrum is primarily composed of HfO_2 with very small contributions from Hf suboxide and HfN components. This is in contrast to spectra (B) and (C) in Fig. 9b and spectrum (4) in Fig. 9a, all of which exhibit substantial Hf suboxide components. These samples were prepared following procedures that yielded switching devices; either by decreasing the purge time [5 s purge time, (4)], or by increasing the deposition temperature [300 °C (B)] or by changing both parameters [300 °C, 5 s purge time (C)]. After analysis of further samples it became clear that a significant presence of Hf suboxides (oxygen vacancies) was required at the interfacial layer with the Ti in order to obtain reproducible hysteretic devices, which is in agreement with previous findings.[46]

XPS analysis of the underlying Ti layer revealed its role as an oxygen and nitrogen gettering agent. Titanium is known for its strong affinity for forming oxygen and nitrogen compounds and

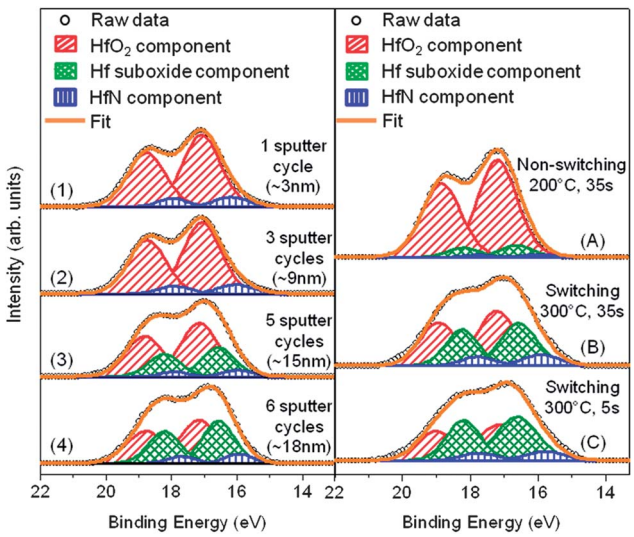

Fig. 9 (a) The evolution of the Hf 4f region, for a hysteretic device fabricated at 200 °C and 5 s purge time, upon sputtering from the surface to the underlying Ti layer. The approximate depth of each profile is also detailed in parentheses. A significant presence of Hf sub-oxide content was found at the Ti interface (after 5 and 6 sputter cycles). (b) The difference in Hf 4f XP spectra in the HfO_{2-x}/Ti interfacial region for different ALD conditions: (A) 200 °C, 35 s purge time (non-hysteretic device), (B) 300 °C, 35 s purge time (hysteretic device), and (C) 300 °C, 5 s purge time (hysteretic device).

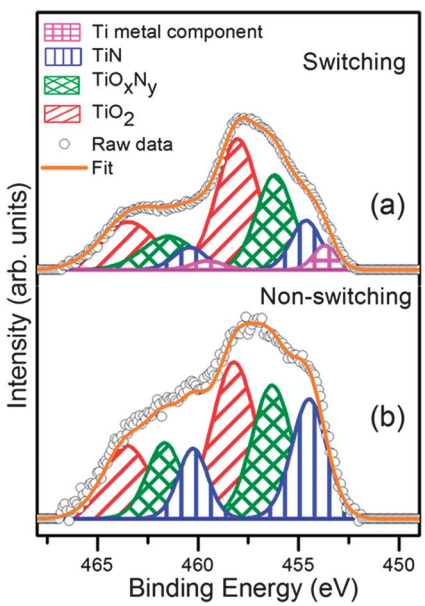

Fig. 10 XPS Ti 2p spectra of (a) a 5 s purge, 200 °C sample (switching device) and (b) a 35 s purge, 200 °C sample (non-switching device). The spectra show the relative increase in nitrogen containing Ti components for the 35 s purged sample.

has been found to act as a getter in similar device structures.[47–49] Fig. 10 shows the Ti 2p XPS spectra from two different samples, one switching (200 °C, 5 s purge time), the other non-switching (200 °C, 35 s purge time). The overall shape of the spectra again exhibits two components due to the Ti $2p_{3/2}$ Ti $2p_{1/2}$ spin orbit doublet. The spectra have been deconvoluted to assign the different Ti species present at the interface, with care to maintain a quantitative fit with the corresponding O 1s and N 1s data. For both samples the interfacial region is found to be composed of titanium oxides, oxynitrides and nitrides with little or no Ti(0) metal detected at the Ti/HfO_2 interface. The Ti $2p_{3/2}$ peak at 453.7 eV in spectrum 10a is characteristic of Ti(0) metal,[50,51] the peak at 454.6 eV corresponds to TiN,[50,52,53] the component at 456.4 is assigned to TiO_xN_y,[50,52,54] and the Ti $2p_{3/2}$ peak at 458.2 eV is typical of amorphous TiO_2.[50,52,54] The presence of Ti(IV) oxide is expected due to the formation of a native oxide layer[55,56] on transferring the sample from the Ti sputter chamber to the ALD chamber during sample preparation, Whereas the detection of titanium nitride and oxynitride species indicates that the Ti layer scavenges oxygen (and nitrogen) from the neighboring HfO_2, generating oxygen vacancies in the interfacial region of the film, which are important for producing resistive switching devices. This capacity to scavenge oxygen from the neighboring HfO_2 could be extended to the HfO_2/Co interface. This assumption lies in the low enthalpy of Co (*i.e.* high oxygen affinity) to react with the HfO_2 bulk and creates oxygen vacancies in the interfacial region. In addition the highly symmetrical *I–V* curve leads us to consider that similar switching behavior can occur at both metal/oxide interfaces.

Further analysis of Fig. 10 shows that the nature of the Ti interfacial layer was also found to depend on the HfO_2 deposition conditions. The spectra show that the sample deposited using a 35 s nitrogen purge time (b) had significantly increased nitrogen containing Ti components, whilst the 5 s purged sample (a) exhibited less nitrogen containing components and still showed a small metallic component.

These results indicate that the HfO_2 deposition conditions have a significant effect on the gettering potential of the underlying Ti, which in turn determines the amount of interfacial Hf sub-oxides present and hence the resistive switching behavior of the device. Long nitrogen purge times cause the Ti layer to saturate, reducing its ability to remove oxygen from the HfO_2 layer. Low deposition temperatures were also found to be detrimental to the oxygen gettering ability of the Ti.

Devices fabricated using a deposition temperature of 125 °C (5 s purge time) did not exhibit hysteresis performance. However, XPS analysis of the Hf 4f region did not show the predominantly HfO_2 interfacial layer observed for other non-hysteretic devices, as highlighted in Fig. S3 (see ESI†). In fact we observed Hf sub-oxides, but more noticeably a significantly higher quantity of nitrogen containing Hf species than in devices deposited at higher temperatures. This was true not only at the interface with the Ti but throughout the HfO_{2-x} film. We propose that at this low reaction temperature either the ALD reaction does not go to completion or the reaction by-products are not removed efficiently resulting in a contaminated film, causing poor device performance.

To finish, the results obtained from the different characterization techniques indicate that the resistive switching mechanism might be based on the modulation of the interfacial resistance. This interface resistance change is a function of the local oxygen vacancy concentration in the interfacial region, where the redistribution of the oxygen vacancies is induced by electric fields.

Conclusions

In summary, we present HfO_2-based metal–insulator–metal devices and analyze the influence of ALD conditions on the RS through the fabrication of 26 different samples. All samples were characterized electrically by the application of *I–V* curves, voltage pulses, minor loops and retention and stability measurements that revealed bipolar RS behavior and confirmed the non-volatile memory capabilities of the device. The RS performance was compared to the HfO_2 ALD conditions with the data presented in a parameter diagram, which shows experimental results with extensive statistics. XPS measurements carried out on specific samples clearly showed that the presence of Hf sub-oxides (oxygen vacancies) at the interface with the Ti was required in order to achieve a stable RS device. Furthermore, XPS established that the oxygen gettering ability of the underlying Ti layer was key in the formation of these Hf sub-oxides. Certain ALD conditions were found to support the formation of HfO_2 sub-oxides, namely increased deposition temperatures and short purge times.

Acknowledgements

The authors would like to thank P. Levy for a critical reading of the manuscript. We also acknowledge funding support from Juan de la Cierva Program JCI-2010-07837 and by projects MAT2009-08494, MAT2010-21156-C03-03 and MAT2012-37638 from the Spanish Ministry of Science, by the Basque Government through Project nos PI2011-1 and IT-621-13 as well as a Marie Curie Reintegration Grant (ITAMOSCINOM) from the European Commission.

Notes and references

1 G. R. Burr, B. N. Kurdi, J. C. Scott, C. H. Lam, K. Gopalakrishnan and R. S. Shenoy, *IBM J. Res. Dev.*, 2008, **52**, 449–464.
2 A. Sawa, *Mater. Today*, 2008, **11**, 28–36.
3 R. Waser and M. Aono, *Nat. Mater.*, 2007, **6**, 833–840.
4 B. P. Andreason, M. Janousch, U. Staub and G. I. Meijer, *Appl. Phys. Lett.*, 2009, **94**, 013513.
5 K. Szot, W. Speier, G. Bihlmayer and R. Waser, *Nat. Mater.*, 2006, **5**, 312–320.
6 M. Janousch, G. I. Meijer, U. Staub, B. Delley, S. F. Karg and B. P. Andreasson, *Adv. Mater.*, 2007, **19**, 2232.
7 S. Karg, G. I. Meijer, D. Widmer and J. G. Bednorz, *Appl. Phys. Lett.*, 2006, **89**, 072106.

8 S. Seo, M. J. Lee, D. H. Seo, E. J. Jeoung, D. S. Suh, Y. S. Joung, I. K. Yoo, I. R. Hwang, S. H. Kim, I. S. Byun, J.-S. Kim, J. S. Choi and B. H. Park, *Appl. Phys. Lett.*, 2004, **85**, 5655.
9 G. S. Park, X. S. Li, D. C. Kim, R. J. Jung, M. J. Lee and S. Seo, *Appl. Phys. Lett.*, 2007, **91**, 222103.
10 I. K. Yoo, B. S. Kang, Y. D. Park, M. J. Lee and Y. Park, *Appl. Phys. Lett.*, 2008, **92**, 202112.
11 J. P. Strachan, M. D. Pickett, J. J. Yang, S. Aloni, A. L. Kilcoyne, G. Medeiros-Ribeiro and R. S. Williams, *Adv. Mater.*, 2010, **22**, 3573–3577.
12 K. M. Kim, G. H. Kim, S. J. Song, J. Y. Seok, M. H. Lee, J. H. Yoon and C. S. Hwang, *Nanotechnology*, 2010, **21**, 305203.
13 D. H. Kwon, K. M. Kim, J. H. Jang, J. M. Jeon, M. H. Lee, G. H. Kim, X. S. Li, G. S. Park, B. Lee and S. Han, *Nat. Nanotechnol.*, 2010, **5**, 148–153.
14 N. Xu, L. X. Sun, X. Liu, D. Han, Y. Wang, R. Han, J. Kang and B. Yu, *Appl. Phys. Lett.*, 2008, **92**, 232112.
15 A. Shih, W. Zhou, J. Qiu, H.-J. Yang, S. Chen, Z. Mi and I. Shih, *Nanotechnology*, 2010, **21**, 125201.
16 Y. C. Yang, F. Pan, Q. Liu, M. Liu and F. Zeng, *Nano Lett.*, 2009, **9**, 1636–1643.
17 H.-Y. Lee, P. S. Chen, C.-C. Wang, S. Maikap, P.-J. Tzeng, C.-H. Lin, L.-S. Lee and M.-J. Tsai, *Jpn. J. Appl. Phys.*, 2007, **46**, 2175–2179.
18 I.-S. Park, K.-R. Kim, S. Lee and J. Ahn, *Jpn. J. Appl. Phys.*, 2007, **46**, 2172–2174.
19 M. Y. Chan, T. Zhang, V. Ho and P. S. Lee, *Microelectron. Eng.*, 2008, **85**, 2420–2424.
20 Y. M. Kim and J. S. Lee, *J. Appl. Phys.*, 2008, **104**, 114115.
21 Y. Wang, Q. Liu, S. Long, W. Wang, Q. Wang, M. Zhang, S. Zhang, Y. Li, Q. Zuo and J. Yang, *Nanotechnology*, 2010, **21**, 045202.
22 P. Gonon, M. Mougenot, C. Vallée, C. Jorel, V. Jousseaume, H. Grampeix and F. El Kamel, *J. Appl. Phys.*, 2010, **107**, 074507.
23 D. M. Hausmann, E. Kim, J. Becker and R. G. Gordon, *Chem. Mater.*, 2002, **14**, 4350–4358.
24 J. C. Hackley and T. Gougousi, *Thin Solid Films*, 2009, **517**, 6576–6583.
25 K. Kukli, T. Pilvi, M. Ritala, T. Sajavaara, J. Luc and M. Leskelä, *Thin Solid Films*, 2005, **491**, 328–338.
26 K. Kukli, M. Ritala, J. Lu, A. Haårsta and M. Leskelä, *J. Electrochem. Soc.*, 2004, **151**, F189–F193.
27 J. Aarik, A. Aidla, A.-A. Kiisler, T. Uustare and V. Sammelselg, *Thin Solid Films*, 1999, **340**, 110–116.
28 http://www.casaxps.com, © Casa software Ltd. 2009.
29 S. Ain, A. O. Adeyeye, S. Y. Chan and C. B. Boothroyd, *J. Phys. D: Appl. Phys.*, 2004, **37**, 2720–2725.
30 J. J. Yang, I. H. Inoue, T. Mikolajick and C. S. Hwang, *MRS Bull.*, 2012, **37**, 131–137.
31 S. Tsui, A. Baikalov, J. Cmaidalka, Y. Y. Sun, Y. Q. Sun, Y. Q. Wang and Y. Y. Xue, *App. Phys. Lett.*, 2004, **85**, 317.
32 A. Sawa, T. Fujii, M. Kawasaki and Y. Tokura, *Appl. Phys. Lett.*, 2004, **85**, 4073–4075.
33 Y. B. Nian, J. Strozier, N. J. Wu, X. Chen and A. Ignatiev, *Phys. Rev. Lett.*, 2007, **98**, 146403.
34 J. J. Yang, M. D. Pickett, X. Li, D. R. Stewart and R. S. Williams, *Nat. Nanotechnol.*, 2008, **3**, 429–433.
35 M.-J. Lee, C. B. Lee, D. Lee, S. R. Lee, M. Chang, J. H. Hur, Y.-B. Kim, C.-J. Kim, D. H. Seo, S. Seo, U.-I. Chung, I.-K. Yoo and K. Kim, *Nat. Mater.*, 2011, **10**, 625–630.
36 H. Y. Le, Y. S. Chen, P. S. Chen, T. Y. Wu, F. Chen, C. C. Wang, P. J. Tzeng, M. J. Tsai and C. Lien, *IEEE Electron Device Lett.*, 2010, **31**, 44–46.
37 K. Xiong, J. Robertson, M. C. Gibson and S. J. Clark, *Appl. Phys. Lett.*, 2005, **87**, 183505.
38 K. Tse, D. Liu, K. Xiong and J. Robertson, *Microelectron. Eng.*, 2007, **84**, 2028–2031.
39 J. Robertson, O. Sharia and A. A. Demkov, *Appl. Phys. Lett.*, 2007, **91**, 132912.
40 X. Wu, D. B. Migas, X. Li, M. Bosman, N. Raghavan, V. E. Borisenko and K. L. Pey, *Appl. Phys. Lett.*, 2010, **96**, 172901.
41 R. Jiang, E. Q. Xie and Z. F. Wang, *J. Mater. Sci.*, 2007, **42**, 7343–7347.
42 G. He, G. W. Meng, L. D. Zhang and M. Liu, *Appl. Phys. Lett.*, 2007, **91**, 232910.
43 G. He, G. W. Meng, L. D. Zhang and M. Liu, *Appl. Phys. Lett.*, 2002, **81**, 3627–3629.
44 C. Vallée, P. Gonon, C. Mannequin, T. Chevolleau, M. Bonvalot, H. Grampeix, C. Licitra, N. Rochat and V. Jousseaume, *J. Vac. Sci. Technol., A*, 2011, **29**, 041512.
45 A. R. Chourasia, J. L. Hickman, R. L. Miller, G. A. Nixon and M. A. Seabolt, *Int. J. Spectrosc.*, 2009, **1**, 439065.
46 C. Walczyk, C. Wenger, D. Walczyk, M. Lukosius, I. Costina, M. Fraschke, J. Dabrowski, A. Fox, D. Wolansky and S. Thiess, *J. Vac. Sci. Technol., B: Nanotechnol. Microelectron.: Mater., Process., Meas., Phenom.*, 2011, **29**, 01AD02.
47 H. Kim, P. C. McIntyre, C. O. Chui, K. C. Saraswat and S. Stemmer, *J. Appl. Phys.*, 2004, **96**, 3467.
48 K.-I. Seo, D.-I. Lee, P. Pianetta, H. Kim, K. C. Saraswat and P. C. McIntyre, *Appl. Phys. Lett.*, 2006, **89**, 142912.
49 L. V. Goncharova, M. Dalponte, T. Gustafsson, O. Celik, E. Garfunkel, P. S. Lysaght and G. Bersuker, *J. Vac. Sci. Technol., A*, 2007, **25**, 261.
50 P. W. Shum, Z. F. Zhou, K. Y. Li and Y. G. Shen, *Mater. Sci. Eng., B*, 2003, **100**, 204–213.
51 M. C. Biesinger, L. W. M. Lau, A. R. Gerson and R. S. C. Smart, *Appl. Surf. Sci.*, 2010, **257**, 887–898.
52 J. F. Marco, J. R. Gancedo, M. A. Auger, O. Sanchez and J. M. Albella, *Surf. Interface Anal.*, 2005, **37**, 1082–1091.
53 I. Bertóti, *Surf. Coat. Technol.*, 2002, **151–152**, 194–203.
54 A. Trenczek-Zajac, M. Radecka, K. Zakrzewska, A. Brudnik, E. Kusior, S. Bourgeois, M. C. Marco de Lucas and L. Imhoff, *J. Power Sources*, 2009, **194**, 93–103.
55 E. McCafferty and J. P. Wightman, *Appl. Surf. Sci.*, 1992, **143**, 92–100.
56 J. Pouilleau, D. Devilliers, F. Garrido, S. Durand-Vidal and E. Mahé, *Mater. Sci. Eng., B*, 1997, **B47**, 235–243.

